

UCLA

UCLA Previously Published Works

Title

Focal cortical dysplasia imaging discrepancies between MRI and FDG-PET: Unique association with temporal lobe location

Permalink

<https://escholarship.org/uc/item/3sj3p4q4>

Authors

Yokota, Hajime
Uetani, Hiroyuki
Tatekawa, Hiroyuki
et al.

Publication Date

2020-10-01

DOI

10.1016/j.seizure.2020.08.017

Peer reviewed



Published in final edited form as:

Seizure. 2020 October ; 81: 180–185. doi:10.1016/j.seizure.2020.08.017.

Imaging Discrepancy between MRI and FDG-PET in Focal Cortical Dysplasia: Unique Association with Temporal Lobe Location

Hajime Yokota¹, Hiroyuki Uetani², Hiroyuki Tatakawa², Akifumi Hagiwara², Emiko Morimoto¹, Michael Linetsky², Bryan Yoo², Benjamin M. Ellingson², Noriko Salamon²

¹Department of Diagnostic Radiology and Radiation Oncology, Graduate School of Medicine, Chiba University, Chiba, Japan

²Department of Radiological Sciences, David Geffen School of Medicine at UCLA, Los Angeles, California, United States

Abstract

BACKGROUND AND PURPOSE: Although MRI and FDG-PET are used for pre-surgical assessment of focal cortical dysplasia, they often disagree. The purpose of this study was to identify factors that contribute to the imaging discrepancy of focal cortical dysplasia between MRI and FDG-PET.

MATERIALS AND METHODS: Sixty-two patients (mean age, 18.9) with a focal cortical dysplasia type I or II were retrospectively selected. These patients were visually categorized into two groups: the extent of PET abnormality larger than MRI abnormality and vice versa or equivalent. Predicting factors of these two groups were analyzed by multivariate logistic regression. The extent of hypometabolic transient zone surrounding focal cortical dysplasias and their mean normalized standardized uptake values were measured and compared using Mann-Whitney U test.

RESULTS: FCDs were detected on MRI and PET in 46 and 55 patients, respectively, whereas no abnormality was detected in 4 patients. The PET hypometabolic areas were larger than the MRI abnormal areas in 26 patients (88% in the temporal lobe), while the PET hypometabolic areas were equivalent or smaller than the MRI abnormal areas in 32 patients (69% in the frontal lobe). The temporal lobe location was an independent predictor to differentiate the two groups (OR = 35.2, 95% CI = 6.81–168.0, $P < .001$). The temporal lobe lesions had significantly wider transient zone and lower standardized uptake values than those in the other lobes (both P s $< .001$).

CONCLUSIONS: Discrepancy between MRI and FDG-PET findings of focal cortical dysplasia was associated with temporal lobe location.

Keywords

Focal cortical dysplasia; MRI; ¹⁸F-FDG PET

INTRODUCTION

Focal cortical dysplasia (FCD) is a common cause of intractable epilepsy that may be amenable to surgical therapy. FCDs are usually evaluated using multimodal structural and functional neuroimaging including MRI, FDG-PET, SPECT, and magnetoencephalograms. Although MRI is the preferred imaging method in the diagnosis of patients with intractable epilepsy, detection of FCD is not always satisfactory, whereas FDG-PET may enable the detection of FCD even in MRI-negative cases.^{1, 2} The sensitivity using MRI was reported to be between 55–80% for the diagnosis of FCD type I and 65–90% for FCD type II.^{3–6} Meanwhile, the sensitivity of FDG-PET was estimated to be between 70–90%.^{2, 3, 7, 8} Because there is trade-off between the extent of resection of epileptogenic zone and post-operative functional status, clear delineation of the extent of FCDs is crucial. However, the results of MRI and FDG-PET often conflict each other, which generates considerable debate regarding presurgical evaluation and interpretation of FCDs, potentially leading to unsatisfactory post-operative outcomes.^{9, 10}

Although the correlations between pathological and imaging findings have been investigated, factors that contribute to the imaging discrepancies of FCDs between MRI and FDG-PET remain uncertain.^{1, 2, 11–14} One potential confounding factor is the location of FCDs. Previous studies have reported associations between the location of FCDs and the pathological subtypes,^{15, 16} and between the location of FCDs and the imaging findings of MRI and FDG-PET;² however, the underlying factors of discrepancies in imaging findings between MRI and FDG-PET have not been determined. Furthermore, these studies were performed only by univariate analyses based on visual assessments. We hypothesized that the mismatch of MRI/PET findings may be associated with the location of FCDs.

Thus, the main purpose of this study was to identify factors that contribute to the imaging discrepancies in imaging findings of FCDs between MRI and FDG-PET. We performed visual and quantitative assessments of FCDs in association with their locations.

MATERIALS AND METHODS

Subjects

The research protocol was approved by the local institutional review board. The requirement of informed consent for this retrospective study was waived. A total of 157 consecutive patients underwent surgery and were pathologically diagnosed with FCD (type I, 43; type II, 52; type III, 62) at our institution between January 2004 and January 2016. Subjects were subsequently excluded if they (i) had FCD type III (62 cases), which included patients with hippocampal sclerosis confirmed by pathological findings if available and/or MRI changes defined as the presence of both hippocampal atrophy and hyperintensity on T2WI; (ii) exhibited FCDs extending into multiple lobes (25 cases); (iii) did not have adequate MRI and FDG-PET data available for presurgical evaluations (7 cases); or (iv) had FDG-PET data acquired only during the ictal phase (1 case).

Neuroimaging

Presurgical MRI and FDG-PET exams were selected so that the period between the two studies were the shortest. MRI was performed on a 1.5-T (Siemens Sonata; Siemens AG, Erlangen, Germany; GE Genesis or GE Signa HDx; GE Healthcare, Milwaukee, Wisconsin, USA), or a 3-T MR scanner (Siemens Trio; Siemens AG, Erlangen, Germany). Structural MRI examinations included a 3D T1-weighted coronal gradient echo sequence (TR/TE = 11–25 ms/3–5 ms, slice thickness = 0.9–1.2 mm), a 2D T2-weighted axial and coronal sequence (TR/TE = 3000–5500 ms/90–130 ms, slice thickness = 4.0 mm), and a 2D FLAIR axial and coronal sequence (TR/TE = 8800–9500 ms/80–125 ms, TI = 2200–2500 ms, slice thickness = 4.0 mm). After a fasting period of more than 6 hours, FDG-PET images were acquired on a Siemens CTI PET scanner or a Siemens TruePoint BioGraph Model 1093 PET/CT scanner with 19 or 34 cm FOV, and 2.5 mm or 1.5 mm slice thickness at 40 min after intravenous injection of ^{18}F -FDG (0.14 mCi/kg). All PET scans were performed during a non-ictal phase, which was established using electroencephalography just prior to the examinations. MRI and FDG-PET images were co-registered using the Oncology Fusion function on a Vitrea workstation (Vital Images) as previously described.¹⁴ According to the standard practice at our institution, PET images were overlaid on T1WI as color maps depicting differences in FDG uptake values in 15% increments. Red color was assigned to the highest FDG uptake value in the striate body. These images were used for the following visual assessment.

Visual Assessment

Abnormal regions on MRI and hypometabolic regions on FDG-PET were visually delineated and compared by two neuroradiologists (XX and YY with 12 and 20 years of experience, respectively). Any discordances between the two readers were settled by consensus. The borders of hypometabolic areas were determined based on the asymmetry to the contralateral hemisphere. FCDs were divided into four groups based on the following evaluations (Fig 1): group A, the hypometabolic area on PET is larger than the abnormal area on MRI; group B, the hypometabolic area on PET is equivalent to the abnormal area on MRI; group C, the hypometabolic area on PET is smaller or less evident than the area of MRI abnormality; and group D, negative for both PET and MRI.

Quantitative Assessment

To corroborate the results of visual assessment, we measured the extent of transient zone (TZ) of FDG hypometabolic area by mathematically defining the boundary of FCDs on FDG-PET. Processing procedures used for quantitative analyses are described in Fig 2. Statistical parametric mapping software (SPM12; Wellcome Trust Centre for Neuroimaging, London, United Kingdom; <https://www.fil.ion.ucl.ac.uk/spm/software/spm12/>) and Analysis of Functional NeuroImages (AFNI; NIMH Scientific and Statistical Computing Core; Bethesda, MD, USA; <http://afni.nimh.nih.gov/afni>) were used for the following analyses. ROIs of MRI abnormalities implying FCD (ROI_{MRI}) were manually drawn for each exam on FLAIR or T2WI. All images of PET, MRI and ROI_{MRI} were linearly registered to the 3D T1WI, and then nonlinearly registered to Montreal Neurological Institute space using the Diffeomorphic Anatomical Registration Through Exponentiated Lie Algebra method

implemented on SPM12. ROI_{MRI} was flipped onto the contralateral healthy hemisphere and a homotopic mirror ROI (mirror ROI_{MRI}) was created on Montreal Neurological Institute space. ROI_{MRI} and mirror ROI_{MRI} were inflated with in a 3D manner for 2 mm width up to 50 mm, and 25 ring-shaped ROIs in total were created. These ring-shaped ROIs were overlaid on the cortical masks, which were thresholded at the GM tissue probability of 0.5. Regions extending to the opposite hemisphere were removed. Finally, 25 peri-ROI_{MRI}s and 25 contralateral mirror peri-ROI_{MRI}s with the distance of 2 mm up to 50 mm from ROI_{MRI} and mirror ROI_{MRI}, respectively, were acquired. ROIs of the striate body were created using the WFU PickAtlas,¹⁷ and the PET images were normalized by dividing the mean SUV of the bilateral striate bodies. The boundary between hypometabolic and normal metabolic areas were mathematically determined at the inflection point of the normalized SUV (nSUV) of peri-ROI_{MRI}. At each level of peri-ROI_{MRI}, the ratio of the mean nSUV of peri-ROI_{MRI} to that of the corresponding mirror peri-ROI_{MRI} was calculated from the closest level (2 mm) to the farthest level (50 mm) of the ROI_{MRI}. When the ratio reached 0.95, one point closer to that level was defined as the inflection point. The threshold value, 0.95, was derived from a previous study that investigated the normal range of laterality of FDG uptake in healthy controls.¹⁸ The distance from the ROI_{MRI} to the inflection point was defined and recorded as the extent of TZ surrounding the ROI_{MRI}.

Statistical Analysis

The patients' characteristics and the results of the visual assessment were compared between the group with the hypometabolic area on PET larger than the abnormal area on MRI (MRI < FDG-PET group [group A]) and the group with the hypometabolic area on PET equivalent to or smaller than the abnormal area on MRI (MRI = FDG-PET group [group B and C]) using Fisher's exact test or Mann-Whitney U test. To identify factors that are associated with larger abnormality on PET than MRI, a multivariate logistic regression analysis was performed. Age at seizure onset, pathological subtypes (type I versus II), and location of FCDs (the temporal lobe versus the other lobes) were selected as independent variables according to clinical importance and the limitations imposed by the number of subjects. For quantitative assessment, the extent of the TZ and the mean nSUV of FCDs were compared between the subgroups determined by visual assessment (MRI < FDG-PET group versus MRI = FDG-PET group), between the different pathological subtypes (type I versus II), and between the subgroups of FCD location (the temporal lobe vs the other lobes) using Mann-Whitney U test. A two-sided *P* value less than .05 was considered statistically significant.

RESULTS

Patient Characteristics

Patient characteristics are described in Table 1. According to the eligibility criteria, a total of 62 patients (mean age \pm standard deviation (SD), 18.9 ± 14.5 ; female/male = 34/28) out of the 157 original FCD patients were included in the current study. The period between MRI and FDG-PET was 1.8 ± 5.7 (mean \pm SD) months. The mean age at seizure onset (\pm SD) was 9.3 ± 10.6 years, with a mean seizure duration (\pm SD) of 9.6 ± 9.3 years. At one year post-surgery follow-up, 33 (53%) patients were free of disabling seizures (Engel class I), 4 (6%) were almost seizure-free (class II), 7 (11%) showed worthwhile improvement (class

III), and 6 (10%) showed no worthwhile improvement (class **IV**).¹⁹ Twelve patients had no follow-up data available. Thirty-two patients (52%) had FCD type I and 30 (48%) had type II. Thirty-four (55%) patients had FCD lesions on the left side. Twenty-four (39%) FCD lesions were localized to the frontal lobe, 29 (47%) to the temporal lobe, 6 (10%) to the parietal lobe, and 2 (3.2%) to the occipital lobe.

Visual Assessment

MRI and FDG-PET enabled detection of FCD lesions in 46 (74%) and 55 (89%) patients, respectively. According to the MRI/PET findings, 26, 29, 3, and 4 FCD patients were included in group A, B, C, and D, respectively. In group A, 23 of 26 (89%) FCD lesions were localized to the temporal lobe. No FCD lesions were localized to the frontal lobe. In group B, 19 of 29 (66%) FCD lesions were localized to the frontal lobe, while only 5 (17%) FCD lesions were localized to the temporal lobe. In group C, all three FCD lesions were localized to the frontal lobe. These three patients showed no abnormality on FDG-PET. No MRI nor FDG-PET abnormalities were detected in four patients and they were categorized as group D. Patients in group D was removed from the subsequent analyses because delineation of such normal appearing lesions was difficult in visual assessment.

When comparing the MRI < FDG-PET and the MRI = FDG-PET groups, age at seizure onset (Mann-Whitney U test, $P = .017$), the pathological subtype of FCDs (Fisher's exact test, $P = .02$), and the location of FCDs (Fisher's exact test, $P < .001$) showed significant differences (Table 2). In a multivariate analysis, the temporal lobe location (OR = 35.2, 95% CI = 6.81–168.0, $P < .001$) was an independent predictor discriminating between the two groups, while neither the age at seizure onset ($P = .85$) nor the pathological subtype ($P = .65$) showed significant differences (Table 3).

Quantitative Assessment

Because 16 FCD lesions (type I, 8, type II, 8; frontal lobe, 5, temporal lobe, 7, parietal lobe, 3, occipital lobe, 1) were not visible on MRI, they were excluded from the quantitative analysis; therefore, 46 FCD patients were included in the quantitative evaluations (type I, 25, type II, 21; frontal lobe, 19, temporal lobe, 22, parietal lobe, 4, occipital lobe, 1).

The results of quantitative assessments are described in Table 4. The TZ was significantly larger in the MRI < FDG-PET group compared to the MRI = FDG-PET group (mean \pm SD, 24.32 ± 12.15 mm vs 10.37 ± 11.78 mm, $P = .002$). The TZ of the temporal lobe lesions (22 lesions) was significantly larger than that of the lesions in the other lobes (19 frontal lobe lesions, 4 parietal lobe lesions, and 1 occipital lobe lesions) (mean \pm SD, 24.36 ± 12.70 mm versus 8.58 ± 9.95 mm, $P < .001$). The mean nSUV of ROI_{MRI} was significantly lower in the MRI < FDG-PET group than the MRI = FDG-PET group (mean \pm SD, 0.59 ± 0.08 versus 0.82 ± 0.18 , $P < .001$). The mean nSUV of the temporal lobe lesions was significantly lower than that of the lesions in the other lobes (mean \pm SD, 0.59 ± 0.08 versus 0.84 ± 0.17 , $P < .001$). Neither the TZ nor the mean nSUV showed significant differences between FCD type I and II.

DISCUSSION

In the current study, factors that contribute to the imaging discrepancies of FCDs between MRI and FDG-PET were investigated by visual assessment, and were corroborated by quantitative assessments. On visual assessment, temporal lobe location was revealed to be a strong factor for predicting the abnormal area on PET being larger than that on MRI. For the quantitative analysis, we mathematically determined the boundaries of hypometabolic areas and calculated the extent of TZ. As a result, FCD lesions in the temporal lobe showed larger TZ and lower nSUV compared to those in the other lobes, which was compatible with visual assessments. Most previous studies evaluated hypometabolic regions with voxel-based morphometry using SPM; however, these analyses needed healthy controls as references, which exposes healthy controls to radiation. In contrast, the analysis of TZ performed in our study does not require healthy controls.

This study revealed that FCDs in the temporal lobe had larger hypometabolic areas on FDG-PET compared with abnormal areas on MRI and lower nSUV than FCDs in the other lobes. Ryvlin *et al.*²⁰ reported that epilepsy patients with cavernous malformation had hypometabolic regions only when the lesion is located in the temporal lobe. The underlying pathophysiology was supposed that the vascular malformation disrupted connections between paralimbic areas and adjacent temporal neocortex where hypometabolism was most pronounced. Similarly, a previous FDG-PET study using SPM revealed that 67% of mesial temporal lobe epilepsy patients had extensive extratemporal hypometabolic areas where were more frequent in the frontal lobe and insula.²¹ Hence, such hypometabolic extension may vary due to various seizure propagation or surrounding connectivity patterns. A previous study reported that the temporal lobe cortex had physiologically lower metabolic activity on FDG-PET compared to the other lobes.²² This may partly explain why FCDs in the temporal lobe showed lower nSUV than FCDs in the other lobes in our study.

In contrast, no FCD lesions in the frontal lobe showed larger hypometabolic areas on FDG-PET than the corresponding MRI abnormal areas; furthermore, all three FCD lesions the showed smaller FDG hypometabolic areas than the MRI abnormal area were localized only to the frontal lobe. There are several possible explanations to these phenomena. First, as discussed above, because the seizure propagation patterns are assumed to depend on the area of seizure onset and its anatomical connections, the frontal lobe localization of FCDs may reflect restricted propagation pattern involving only the neighboring zone compared to the FCDs in the temporal lobe.²³ Second, most FCDs in the frontal lobe were reported to be located at the bottom of deep sulci and connected to the superficial normal-appearing cortex, whereas FCDs in the temporal lobe often involved the temporal tip.²⁴ Such locational or morphological differences may cause the results of the hypometabolic area on FDG-PET equivalent to or smaller than the abnormal area on MRI in the frontal lobe FCDs.

Limitations of this study included its retrospective design, and variability in acquisition protocols and instruments over time. The latter was mainly due to technological advances in PET and MRI systems evolving during the study period. We mitigated the variability by normalizing SUV. Another limitation of the study was the absence of a control population;

however, including healthy controls in this study was not ethical due to the radiation exposure by FDG-PET examinations.

Conclusions

The temporal location of FCD lesions was revealed to be the major predicting factor of the larger area of abnormality on FDG-PET than MRI.

ABBREVIATIONS:

FCD	focal cortical dysplasia
nSUV	normalized SUV
SD	standard deviation
TZ	transient zone

References

1. Chugani HT, Conti JR. Etiologic classification of infantile spasms in 140 cases: role of positron emission tomography. *Journal of child neurology* 1996;11:44–48 [PubMed: 8745385]
2. Halac G, Delil S, Zafer D, et al. Compatibility of MRI and FDG-PET findings with histopathological results in patients with focal cortical dysplasia. *Seizure* 2017;45:80–86 [PubMed: 27960132]
3. Lerner JT, Salamon N, Hauptman JS, et al. Assessment and surgical outcomes for mild type I and severe type II cortical dysplasia: a critical review and the UCLA experience. *Epilepsia* 2009;50:1310–1335 [PubMed: 19175385]
4. Krsek P, Maton B, Korman B, et al. Different features of histopathological subtypes of pediatric focal cortical dysplasia. *Annals of neurology* 2008;63:758–769 [PubMed: 18571798]
5. Alshafai L, Ochi A, Go C, et al. Clinical, EEG, MRI, MEG, and surgical outcomes of pediatric epilepsy with astrocytic inclusions versus focal cortical dysplasia. *Epilepsia* 2014;55:1568–1575 [PubMed: 25169867]
6. Colombo N, Salamon N, Raybaud C, et al. Imaging of malformations of cortical development. *Epileptic Disord* 2009;11:194–205 [PubMed: 19720583]
7. Kim DW, Lee SK, Chu K, et al. Predictors of surgical outcome and pathologic considerations in focal cortical dysplasia. *Neurology* 2009;72:211–216 [PubMed: 19005176]
8. Park CK, Kim SK, Wang KC, et al. Surgical outcome and prognostic factors of pediatric epilepsy caused by cortical dysplasia. *Childs Nerv Syst* 2006;22:586–592 [PubMed: 16541293]
9. Thom M, Mathern GW, Cross JH, et al. Mesial temporal lobe epilepsy: How do we improve surgical outcome? *Annals of neurology* 2010;68:424–434 [PubMed: 20976764]
10. Vinton AB, Carne R, Hicks RJ, et al. The extent of resection of FDG-PET hypometabolism relates to outcome of temporal lobectomy. *Brain* 2007;130:548–560 [PubMed: 16959818]
11. Blumcke I, Thom M, Aronica E, et al. The clinicopathologic spectrum of focal cortical dysplasias: a consensus classification proposed by an ad hoc Task Force of the ILAE Diagnostic Methods Commission. *Epilepsia* 2011;52:158–174 [PubMed: 21219302]
12. Guerrini R, Duchowny M, Jayakar P, et al. Diagnostic methods and treatment options for focal cortical dysplasia. *Epilepsia* 2015;56:1669–1686 [PubMed: 26434565]
13. Madan N, Grant PE. New directions in clinical imaging of cortical dysplasias. *Epilepsia* 2009;50 Suppl 9:9–18
14. Salamon N, Kung J, Shaw SJ, et al. FDG-PET/MRI coregistration improves detection of cortical dysplasia in patients with epilepsy. *Neurology* 2008;71:1594–1601 [PubMed: 19001249]

15. Mellerio C, Labeyrie MA, Chassoux F, et al. Optimizing MR imaging detection of type 2 focal cortical dysplasia: best criteria for clinical practice. *AJNR Am J Neuroradiol* 2012;33:1932–1938 [PubMed: 22555587]
16. Bartolini L, Whitehead MT, Ho CY, et al. Temporal lobe epilepsy and focal cortical dysplasia in children: A tip to find the abnormality. *Epilepsia* 2017;58:113–122 [PubMed: 27864929]
17. Maldjian JA, Laurienti PJ, Kraft RA, et al. An automated method for neuroanatomic and cytoarchitectonic atlas-based interrogation of fMRI data sets. *Neuroimage* 2003;19:1233–1239 [PubMed: 12880848]
18. Peter J, Khosravi M, Werner TJ, et al. Global temporal lobe asymmetry as a semi-quantitative imaging biomarker for temporal lobe epilepsy lateralization: A machine learning classification study. *Hellenic journal of nuclear medicine* 2018;21:95–101 [PubMed: 30006642]
19. Engel JJ, Van Ness PC, Rasmussen TB, et al. Outcome with respect to epileptic seizures. In: Engel J Jr, ed. *Surgical treatment of the epilepsies*. 2nd ed. New York: Raven Press; 1993:609–21
20. Ryvlin P, Mauguiere F, Sindou M, et al. Interictal cerebral metabolism and epilepsy in cavernous angiomas. *Brain* 1995;118 (Pt 3):677–687 [PubMed: 7600085]
21. Wong CH, Bleasel A, Wen L, et al. The topography and significance of extratemporal hypometabolism in refractory mesial temporal lobe epilepsy examined by FDG-PET. *Epilepsia* 2010;51:1365–1373 [PubMed: 20384730]
22. Pourhassan Shamchi S, Khosravi M, Taghvaei R, et al. Normal patterns of regional brain (18)F-FDG uptake in normal aging. *Hellenic journal of nuclear medicine* 2018;21:175–180 [PubMed: 30411727]
23. Jenssen S, Roberts CM, Gracely EJ, et al. Focal seizure propagation in the intracranial EEG. *Epilepsy Res* 2011;93:25–32 [PubMed: 21130604]
24. Besson P, Andermann F, Dubeau F, et al. Small focal cortical dysplasia lesions are located at the bottom of a deep sulcus. *Brain* 2008;131:3246–3255 [PubMed: 18812443]

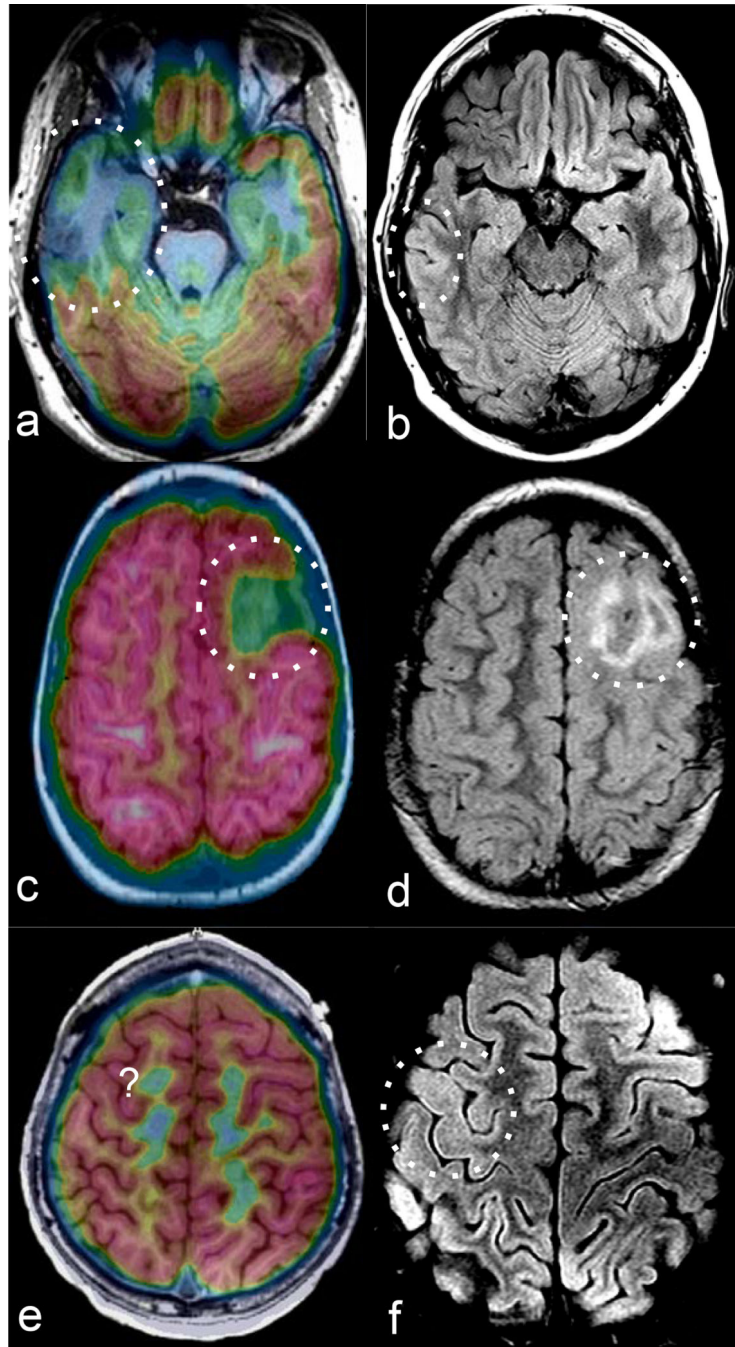
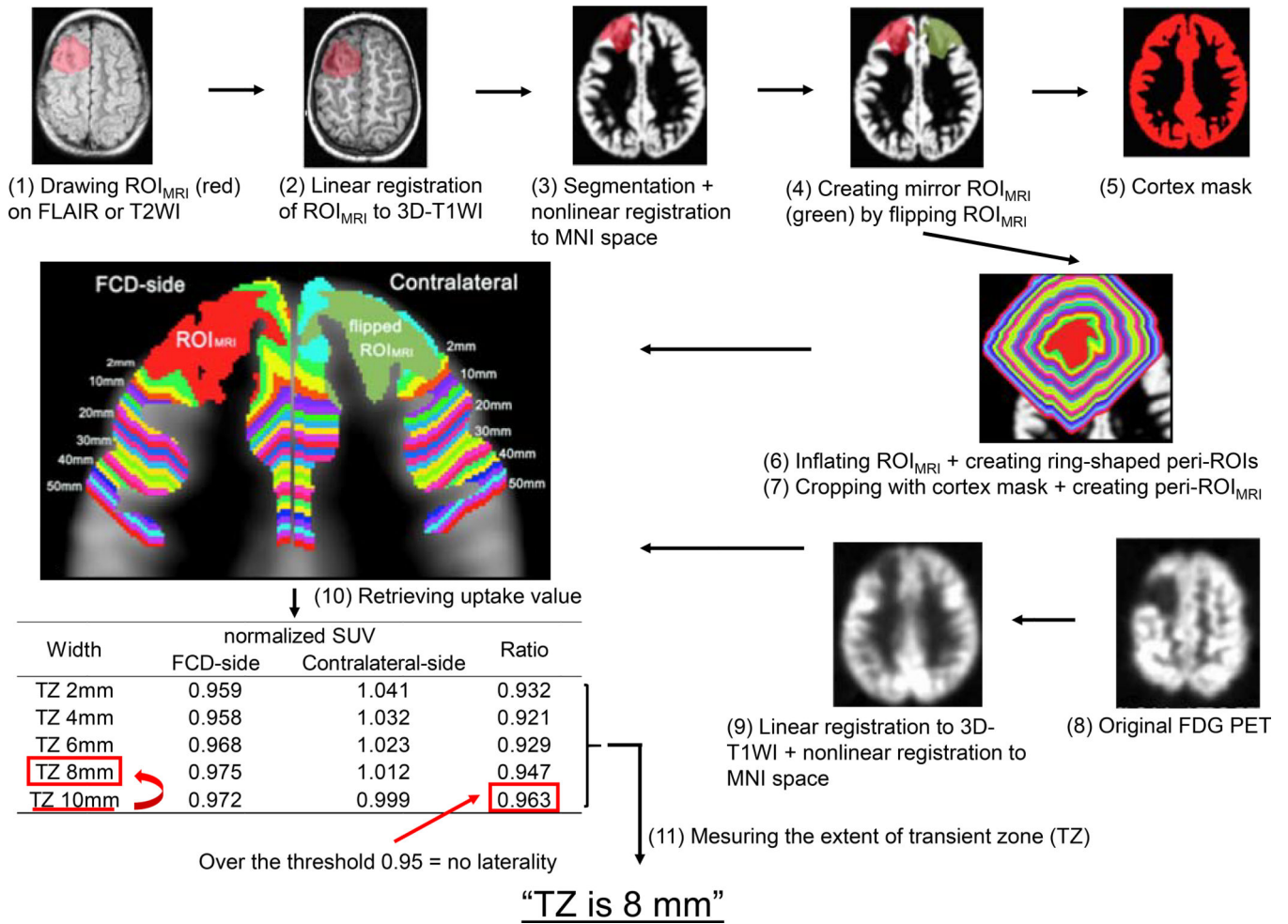


Fig 1. Visual assessment. The hypometabolic area on PET (a, dotted circle) is larger than the abnormal area on MRI (b, dotted circle). This is a FCD type I in the right anterior temporal lobe and categorized as Group A. The hypometabolic area on PET (c, dotted circle) is equal to the MRI abnormal area (d, dotted circle). This is a FCD type IIb in the left superior and middle frontal gyrus and categorized as Group B. The hypometabolic area on PET (e) is subtle, while the MRI abnormality is evident (f, dotted circle). This is a FCD type I in the right precentral gyrus and categorized as Group C.

**Fig 2.**

Post-processing method. (1) ROI of abnormality on MRI implying FCD (ROI_{MRI}) is manually drawn on FLAIR or T2WI. (2) An ROI_{MRI} is linearly registered to the 3D T1WI. (3) GM and WM are segmented. Then the ROI_{MRI} and GM images are nonlinearly registered to the Montreal Neurological Institute space using the Diffeomorphic Anatomical Registration Through Exponentiated Lie Algebra method. (4) Homotopic mirror ROI (mirror ROI_{MRI}) is created by flipping ROI_{MRI} to the contralateral healthy hemisphere on the Montreal Neurological Institute space. (5) A cortical mask is created using the GM segmentation data by thresholding at the tissue probability of 0.5. (6) ROI_{MRI} and mirror ROI_{MRI} are inflated with 2 mm width up to 50 mm. Within each inflated region, 25 ring-shaped concentric perilesional ROIs are created in a 3D manner. (7) All ROIs are cropped with the cortical mask and regions extending to the contralateral hemisphere are removed. Then, peri-ROI_{MRI} and mirror-peri-ROI_{MRI} are created. (8, 9) Similarly, FDG-PET images are registered to the 3D T1WI and nonlinearly registered to Montreal Neurological Institute space. (10) All ROIs (peri-ROI_{MRI} and mirror-peri-ROI_{MRI}) are superimposed to FDG-PET images. (11) Mean values of the normalized SUV (nSUV) relative to the striatum are extracted from each peri-ROI_{MRI} and mirror-peri-ROI_{MRI}, and compared at each level. The ratio of the mean nSUV within a peri-ROI_{MRI} to the mean nSUV within the corresponding

mirror-peri-ROI_{MRI} is calculated at each level from the closest level (2 mm) to farthest level (50 mm). When the ratio of the mean nSUV reaches the threshold of 0.95, one point closer to the ROI_{MRI} is defined as the inflection point. The distance between the ROI_{MRI} and inflection point is defined as the extent of the transient zone surrounding the ROI_{MRI}.

Table 1.

Patient characteristics and visual assessments

		Total (n = 62)	group A (n = 26)	group B (n = 29)	group C (n = 3)	group D (n = 4)
Age, mean ± SD		18.9 ± 14.5	22.4 ± 13.9	15.7 ± 14.1	22.7 ± 15.9	22 ± 20.3
Female, n (%)		34 (54.8)	15 (57.7)	16 (55.1)	0 (0)	3 (75)
Age at seizure onset, mean ± SD		9.3 ± 10.6	11.7 ± 10.5	6.5 ± 8.7	3.3 ± 3.1	16.5 ± 20.0
Seizure duration, mean ± SD		9.6 ± 9.3	10.7 ± 9.3	9.2 ± 10.1	19.3 ± 13.7	5.5 ± 4.0
History of status epilepticus, n (%)		6 (9.7)	3 (11.5)	2 (6.9)	0 (0)	1 (25)
History of primary and secondary generalized seizure, n (%)		22 (35.5)	11 (42.3)	8 (27.6)	0 (0)	3 (75)
Engel class at one year after surgery, n (%)	I	33 (53.2)	13 (50)	16 (55.2)	1 (33.3)	3 (75)
	II–IV	17 (27.4)	6 (23.1)	8 (27.6)	2 (66.7)	1 (25)
	Unknown	12 (19.4)	7 (26.9)	5 (17.2)	0 (0)	0 (0)
Pathological subtype of FCD, n (%)	Type I	32 (51.6)	18 (69.2)	11 (37.9)	1 (33.3)	2 (50)
	Type II	30 (48.4)	8 (30.8)	18 (62.1)	2 (66.7)	2 (50)
Laterality of FCD, n (%)	Left	34 (54.8)	17 (65.4)	14 (48.3)	1 (33.3)	2 (50)
	Right	28 (45.2)	9 (34.6)	15 (51.7)	2 (66.7)	2 (50)
Location of FCD, n (%)	Frontal	24 (38.7)	0 (0)	19 (65.5)	3 (100)	2 (50)
	Temporal	29 (46.8)	23 (88.4)	5 (17.2)	0 (0)	1 (25)
	Parietal	7 (11.3)	2 (7.7)	4 (13.8)	0 (0)	1 (25)
	Occipital	2 (3.2)	1 (3.8)	1 (3.4)	0 (0)	0 (0)

Note:— group A, the hypometabolic area on PET is larger than the abnormal area on MRI; group B, the hypometabolic area on PET is equivalent to the abnormal area on MRI; group C, the hypometabolic area on PET is smaller or less evident than the area of MRI abnormality; and group D, negative for both PET and MRI.

Table 2.

Visual assessment of the factors associated with MRI/FDG-PET imaging discrepancies

	MRI/FDG-PET imaging discrepancy			<i>P</i> value
	MRI < FDG-PET (n = 26)	MRI	FDG-PET (n = 32)	
Female, n (%)	15 (57.7)		16 (50)	.605 ^a
Age at seizure onset, mean ± SD	11.7 ± 10.5		6.5 ± 8.7	.017 ^b
Seizure duration, mean ± SD	10.7 ± 9.3		9.2 ± 10.1	.13 ^b
History of status epilepticus, n (%)	3 (11.5)		2 (6.3)	.65 ^a
History of primary and secondary generalized seizure, n (%)	11 (42.3)		8 (25)	.26 ^a
Engel class at one year after surgery, n (%)	I	13 (50)	17 (53.1)	.76 ^a
	II–IV	6 (26.1)	10 (31.3)	
Pathological type of FCD, n (%)	Type I	18 (69.2)	12 (37.5)	.02 ^a
	Type II	8 (30.8)	20 (62.5)	
Laterality of FCD, n (%)	Left	17 (65.4)	15 (46.9)	.19 ^a
	Right	9 (34.6)	17 (53.1)	
Location of FCD, n (%)	Frontal	0 (0)	22 (68.8)	< .001 ^a
	Temporal	23 (88.4)	5 (15.6)	
	Parietal	2 (7.7)	4 (12.5)	
	Occipital	1 (3.8)	1 (3.1)	

Note:—

^a tested using the Fisher's exact test.^b tested using the Mann–Whitney U test.

Table 3.

Multivariate logistic regression analysis to predict if the abnormality on FDG-PET is larger than that on MRI

	OR	95% CI	P value
Age at seizure onset	1.01	0.93–1.09	.85
Pathological subtype of FCD (I vs II)	0.70	0.14–3.36	.65
Location (the temporal lobe vs the other lobes)	35.2	6.81–182.0	< .001

Author Manuscript

Author Manuscript

Author Manuscript

Author Manuscript

Table 4

Quantitative assessment of 46 FCD patients

	The extent of the transient zone (mm)		Normalized SUV of FCD	
	Mean \pm SD	<i>P</i> value	Mean \pm SD	<i>P</i> value
Visual assessment subgroup		.002		< .001
MRI < FDG-PET	24.32 \pm 12.15		0.59 \pm 0.08	
MRI = FDG-PET	10.37 \pm 11.78		0.82 \pm 0.18	
Pathological subtype of FCD		.14		.56
Type I	19.52 \pm 14.80		0.70 \pm 0.15	
Type II	12.10 \pm 11.29		0.76 \pm 0.22	
Location		< .001		< .001
The temporal lobe	24.36 \pm 12.70		0.59 \pm 0.08	
The other lobes	8.58 \pm 9.95		0.84 \pm 0.17	